JOURNAL OF CATALYSIS 126, 57–72 (1990)

Adsorption and Catalysis on Silicon-Modified W(110) Surfaces[1]

ALLEN G. SAULT AND D. WAYNE GOODMAN

Fuel Sciences Division 6211, Sandia National Laboratories, Albuquerque, New Mexico 87185; and Department of Chemistry, Texas A&M University, College Station, Texas 77843

Received December 7, 1989; revised March 14, 1990

The adsorption of CO, hydrogen, and benzene was studied at 120 K on silicon-covered W(110) surfaces using temperature-programmed desorption. The saturation coverage of virgin CO is reduced from 0.80 monolayer (ML) on the clean W(110) surface to 0.40 ML in the presence of 0.30 ML of silicon and to 0.21 ML in the presence of 0.56 ML of silicon. No CO adsorption occurs on W(110) covered by a monolayer of silicon. Dissociation of hydrogen, CO, and benzene is strongly inhibited by silicon. The inhibition of CO and hydrogen adsorption by silicon is discussed in terms of the proposed overlayer structures for silicon on W(110). Upon annealing silicon overlayers to 1050 K, silicon diffuses into the bulk to form tungsten silicide, and the resulting increase in the concentration of tungsten atoms at the surface increases the ability of the surface to adsorb CO. Results are compared to those from adsorption studies on silicon-covered polycrystalline tungsten and on a nickeldisilicide surface. The dehydrogenation and hydrogenolysis of cyclohexane were used to test the catalytic properties of the silicon-modified surfaces. Tungsten silicide appears to be a highly selective catalyst for the dehydrogenation of cyclohexane. Comparison with a study of cyclohexane reactions over silane-treated nickel catalysts indicates that high selectivity for dehydrogenation may be a general attribute of silicon-modified metal catalysts. The activity of tungsten silicide for cyclohexane dehydrogenation to benzene is at least as great as that of the Ru(0001) surface. © 1990 Academic Press, Inc.

1. INTRODUCTION

In general, clean tungsten surfaces are poor catalysts due to the extremely high reactivity they display. While tungsten surfaces are capable of breaking a large number of chemical bonds, the resulting molecular fragments are bound too tightly to the surface to allow recombination into useful products. In order to develop tungsten-based catalysts, the reactivity of tungsten surfaces must therefore be moderated. One method of moderation involves addition of a second element to tungsten. For instance, a number of studies have shown that addition of carbon or nitrogen to form tungsten carbides or nitrides results in improved catalytic properties (*1–5*). In addition, tungsten–nickel catalysts have found practical application as hydrodesulfurization catalysts. One of the major goals of investigations of modified tungsten surfaces is the development of catalysts to replace the group VIII metals currently in use as hydrocarbon processing catalysts. The lower cost and wider availability of tungsten compared to those of metals such as platinum or palladium could result in substantial reductions in processing costs if the search for tungsten-based catalysts is successful.

One class of modifiers which has not been extensively investigated on tungsten is semiconductors (*6*), even though the modification of other metals by addition of semiconductors has resulted in surfaces which exhibit interesting catalytic properties (*7–13*). Furthermore, Boudart (*7*) has pointed out that the high thermal stability of silicides and their resistance to sulfiding are desirable characteristics for a catalyst. We have therefore undertaken a study of the chemisorptive and catalytic properties of

[1] This work was performed at Sandia National Laboratories, which is operated for the US Department of Energy under Contract DE-AC04-76D00789.

0021-9517/90 $3.00
Copyright © 1990 by Academic Press, Inc.
All rights of reproduction in any form reserved.

silicon-modified W(110) surfaces. In a previous paper (*14*), the formation of thin silicon and silicide films on W(110) by dissociation of silane was reported. Here, the results of an investigation into the chemisorption of CO, H_2, and benzene on silicon and silicide overlayers on W(110) are presented. These chemisorption experiments demonstrate that silicon-modified tungsten surfaces are much less reactive than clean W(110). The successful moderation of the chemisorptive properties of W(110) by silicon suggests that the catalytic properties of tungsten might also be moderated. In order to test this possibility, the catalytic activity of silicon-modified tungsten surfaces for reactions of cyclohexane with hydrogen was investigated. This particular reaction system was chosen because of an earlier report indicating that silane-treated nickel catalysts show high selectivity for dehydrogenation of cyclohexane vs hydrogenolysis (*9*). This high selectivity is attributed to the inability of nickeldisilicide to dissociate hydrogen (*8*). Similarities between the chemisorption of hydrogen on silicon-modified W(110) surfaces and that on a nickeldisilicide surface (*8*) suggest that tungsten silicides might also show high selectivity for dehydrogenation. In addition, kinetic data for cyclohexane dehydrogenation and hydrogenolysis on Ru(0001) are available (*15*), thereby allowing a direct comparison of the activity of silicon-modified tungsten with that of a group VIII metal.

2. METHODS

The experiments were performed in two separate ion-pumped ultrahigh vacuum (UHV) chambers. The first chamber (*16*) contains facilities for Auger electron spectroscopy (AES), low-energy electron diffraction (LEED), and temperature-programmed desorption (TPD). The mass spectrometer used for TPD is multiplexed to allow up to 15 masses to be monitored simultaneously. A collimating aperture located in front of the mass spectrometer ionizer allows desorption from the back and sides of the crystal and the crystal supports to be excluded from the TPD curves.

A leak valve with a thin needle connected to the outlet was used for CO, H_2, and C_6D_6 exposures. By measuring the pressure change in a calibrated volume on the inlet side of the leak valve, the total number of molecules admitted into the chamber could be calculated. From knowledge of the crystal dimensions and distance from the crystal to the doser, the fraction of admitted molecules intercepted by the surface could also be calculated (*17*). Multiplying this fraction by the total amount of gas admitted gave exposures directly. All CO, H_2, and C_6D_6 exposures are reported as the number of incident molecules per square centimeter.

The second chamber, which has also been described previously (*18*), contains an Auger spectrometer, a mass spectrometer, and a high-pressure reactor (1–1000 Torr) which allows the crystal to be isolated from the main vacuum chamber and exposed to reactant gas mixtures at high pressures. Cyclohexane dehydrogenation and hydrogenolysis on the silicon-modified W(110) surface were studied at 630 K, with 1 Torr cyclohexane and 100 Torr hydrogen. The reactor was run in a batch mode. These reaction conditions are identical to those used in a recent study of cyclohexane reactions on Ru(0001) (*15*), thereby allowing a direct comparison of the catalytic activity of silicon-modified tungsten with that of ruthenium. Reaction products were analyzed using a gas chromatograph (GC) equipped with a flame ionization detector and a 6-ft 10% Carbowax 400 on Chromosorb WHP column obtained from Alltech Associates. Benzene formation rates for the silicon-modified tungsten surfaces are reported as turnover frequencies (TOF), defined as the number of benzene molecules formed per surface tungsten atom per second. The distribution of alkanes produced by hydrogenolysis was not measured since the Carbowax column could not separate alkanes. From the total area under the alkane peak, however, the number of cyclohexane molecules which underwent hydrogenolysis could be calcu-

lated. Hydrogenolysis rates are reported as the number of cyclohexane molecules undergoing hydrogenolysis per surface tungsten atom per second. The density of surface tungsten atoms for the silicon-modified surfaces is assumed to be equal to the tungsten atom density for the clean W(110) surface (1.41×10^{15} cm^{-1}). This may be a poor assumption for the silicide surfaces, but the detailed structure, and therefore the tungsten atom density, of the silicide surfaces is unknown (*14*). The reactor was operated in a differential mode such that the total conversion of cyclohexane to products was always less than 1%.

Silicon overlayers were prepared by dissociation of silane. The formation and characterization of these overlayers are discussed elsewhere (*14*). The silicon coverages and overlayer structures relevant to this study are summarized briefly in Section 3.1.

The W(110) crystals (Metal Crystals Ltd.) were cut and polished on both sides using standard techniques. The main impurity in the crystals was carbon, which was removed by repeated cycles of heating to 1900 K in 1×10^{-8} Torr of oxygen for 1 to 2 min, followed by flashing to 2300 K to remove adsorbed oxygen. After cleaning, only small amounts of carbon could be seen in the Auger spectrum, and the crystals displayed very sharp (1×1) LEED patterns. Oxygen (Matheson, Research Purity), carbon monoxide (Alphagaz, 99.99%), and silane (Matheson, Semiconductor Purity) were used as received. C_6D_6 (MSD Isotopes, 99.6% D) was thoroughly degassed prior to use. Hydrogen (Alphagaz, 99.9999%) was used as received for the thermal desorption studies. For the high-pressure reaction experiments the hydrogen was purified by passing it through a palladium alloy diffusion device (Matheson, Model 8371V) and a liquid nitrogen-cooled trap.

3. RESULTS

3.1. CO Adsorption on Silicon Overlayers

Adsorption of CO on clean W(110) at 120 K results in population of a virgin molecular adsorption state with a maximum coverage of 0.8 monolayers (*19–21*). One monolayer (ML) is defined as a coverage equal to the number density of surface atoms on the W(110) surface (1.41×10^{15} cm^{-2}). During thermal desorption approximately 0.5 ML of the virgin CO is converted to a molecularly adsorbed state known as α-CO, which desorbs near 400 K, while the remainder of the CO molecules undergo dissociation. Recombination of the resulting carbon and oxygen atoms occurs in the range of 900–1200 K (β-CO) (*19–21*). By comparison of the CO desorption peak areas from the silicon-covered surfaces with CO desorption peak areas for clean W(110), the absolute coverages of both α- and β-CO on the silicon-covered surfaces were determined. Saturation CO coverages reported here are reproducible to ±10%.

CO adsorption was studied at 120 K on six different silicon-covered W(110) surfaces: 0.30 ML annealed to 700 K, 0.30 ML annealed to 1050 K, 0.56 ML annealed to 700 K, 0.56 ML annealed to 1050 K, 1.0 ML of silicon annealed to 700 K, and 1.0 ML of silicon annealed to 1050 K. Annealing to 700 K after dissociation of silane removes hydrogen from the surface and results in the formation of ordered overlayer structures (*14*). A quarter monolayer ML of silicon annealed to 700 K forms a $\begin{pmatrix}1 & 1\\ 2 & -2\end{pmatrix}$ structure (Fig. 1a). For a half monolayer of silicon annealed to 700 K, a $\begin{pmatrix}2 & 2\\ 1 & -1\end{pmatrix}$ LEED pattern is observed (Fig. 1b). As the silicon coverage is increased above 0.5 ML, a $\begin{pmatrix}2 & 2\\ 2 & -2\end{pmatrix}$ LEED pattern begins to emerge (Fig. 1c). For a monolayer of silicon annealed to 700 K a disordered $p(2 \times 2)$ LEED pattern is observed (Fig. 1d). The disorder is caused by diffusion of a small amount of silicon into the substrate upon annealing, resulting in slightly less than a full monolayer of silicon being present on the surface.

Annealing silicon overlayers to 1050 K results in diffusion of silicon into the tungsten substrate and reaction between silicon and tungsten to form tungsten silicides (*14*). For silicon coverages less than 0.40 ML, the silicide LEED pattern is quite complex,

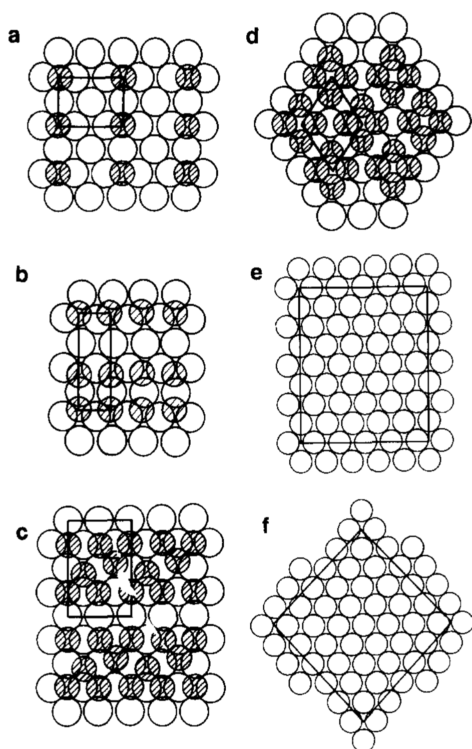

FIG. 1. Overlayer structures for silicon on W(110), from Ref. (*14*). (a) $\begin{pmatrix}1 & 1\\ 2 & -2\end{pmatrix}$ structure for 0.25 ML of silicon; (b) $\begin{pmatrix}2 & 2\\ 1 & -1\end{pmatrix}$ structure for 0.5 ML of silicon; (c) $\begin{pmatrix}2 & 2\\ 2 & -2\end{pmatrix}$ structure observed for 0.75 ML of silicon; (d) $p(2 \times 2)$ structure observed for a monolayer of silicon. Open circles represent tungsten atoms and hatched circles represent silicon atoms. The relative sizes of the tungsten and silicon atoms are taken from Ref. (*39*). (e) Unit cell of $\begin{pmatrix}4 & 4\\ 5 & -5\end{pmatrix}$ silicide structure; (f) unit cell of $\begin{pmatrix}6 & -1\\ -1 & 6\end{pmatrix}$ silicide structure.

consisting of a superposition of at least two different LEED patterns. No adequate solution of this LEED pattern has been found to date. For higher silicon coverages, the LEED patterns are still complex, but determination of the real space unit cells is possible. The silicide overlayer forms a $\begin{pmatrix}4 & 4\\ 5 & -5\end{pmatrix}$ structure for 0.5–0.9 ML of silicon and a $\begin{pmatrix}6 & -1\\ -1 & 6\end{pmatrix}$ structure for a monolayer of silicon (Figs. 1e and 1f). Both of these LEED patterns correspond to very large unit cells, making a determination of the location of the atoms within the unit cells difficult.

The sticking probability of CO, calculated from the known CO exposures and coverages, is of order one on all silicon-covered surfaces, as well as on clean W(110). Sticking probabilities do not vary with CO coverage. No changes in the LEED patterns were observed upon adsorption of CO, except for small increases in the background signal.

3.1.1. β-CO formation. For silicon coverages of 0.56 and 1.0 ML, annealed to either 700 K or 1050 K, filling of the β-CO states is completely suppressed as evidenced by the absence of CO desorption in the range 900–1200 K. For 0.30 ML of silicon, however, some β-CO is formed as shown by the desorption peaks at 900–1200 K in Fig. 2. For 0.30 ML annealed to 700 K approximately 0.16 ML of β-CO is formed following a saturation CO dose. After annealing to 1050 K to form the silicide, the maximum amount of β-CO which can be formed decreases to 0.08 ML.

3.1.2. α-CO formation. In addition to the β-CO states, filling of the α-CO states is also observed in the presence of 0.30 ML of silicon. Figure 2 shows that at saturation, approximately 0.24 ML of CO desorbs at 400 K from a surface covered by 0.30 ML of silicon annealed to 700 K. The desorption temperature of 400 K is nearly identical to the desorption temperature of α-CO from

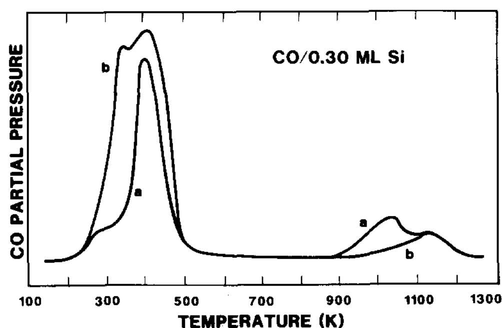

FIG. 2. Thermal desorption of CO from 0.30 ML of silicon on W(110) annealed to (a) 700 K and (b) 1050 K. The adsorption temperature is 120 K. The curves represent a saturation exposure of 9.6×10^{15} cm^{-2} in both cases. The heating rate was not constant over the temperature range, varying from 18 K/s at 200–600 K to 9 K/s at 900–1300 K.

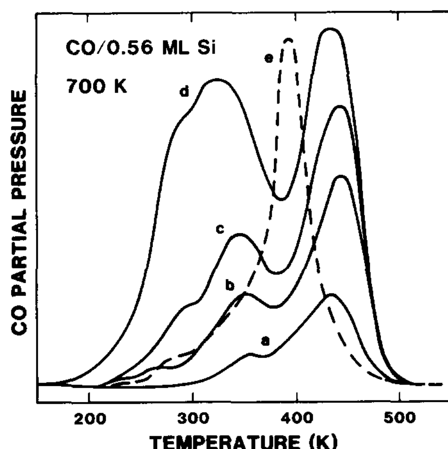

FIG. 3. Thermal desorption of CO from 0.56 ML of silicon on W(110), annealed to 700 K. The adsorption temperature is 120 K. CO exposures are (a) 1.0, (b) 3.9, (c) 5.9, (d) 10.0 × 10^{14} molecules/cm^2. Curve e shows the saturation α-CO TPD from clean W(110) (×1/7). Heating rate = 18 K/s.

clean W(110), indicating that the low-temperature CO desorption shown in Fig. 2 is also due to molecularly adsorbed α-CO. After annealing to 1050 K, the capacity of the surface to form α-CO increases to approximately 0.50 ML (Fig. 2b).

Desorption of CO from a surface covered by 0.56 ML of silicon annealed to 700 K is shown in Fig. 3 for various CO exposures. The saturation CO coverage on this surface is 0.21 ML. Three features are observed in the TPD spectra at 440 K, 350 K, and 280 K. The 350 K feature shifts to slightly lower temperatures as the CO coverage is increased. The three features fill approximately sequentially.

After annealing 0.56 ML of silicon to 1050 K the CO desorption spectra shows only two peaks at 440 and 350 K (Fig. 4), which fill sequentially as the CO dose is increased. A maximum CO coverage of 0.50 ML is obtained on this surface following a CO exposure of 4.0 × 10^{15} molecules/cm^2. As for the lower silicon coverage, the similarity between the CO desorption temperatures in Figs. 3 and 4, and the α-CO desorption temperature for clean W(110), indicates that the CO desorption shown in Figs. 3 and 4 is due to molecularly adsorbed α-CO.

CO adsorption is almost completely suppressed by the presence of a monolayer of silicon annealed to 700 K. The CO TPD shows only a single small peak at 475 K which corresponds to a CO coverage on the order of 0.01 ML. After annealing the silicon monolayer to 1050 K, a saturation coverage of 0.12 ML can be obtained after a 2.0 × 10^{15} molecule/cm^2 exposure. This CO desorbs in three peaks with temperatures of 410, 480, and 540 K, as shown in Fig. 5. Again, these desorption peaks are due to molecularly adsorbed α-CO.

3.2. Hydrogen Adsorption on Silicon Overlayers

Hydrogen adsorption was studied at 120 K on four different surfaces: 0.5 ML of silicon annealed to 700 K, 0.5 ML of silicon annealed to 1050 K, one monolayer of silicon annealed to 700 K, and one monolayer of silicon annealed to 1050 K. Hydrogen coverages were calibrated by comparison with the saturation H_2 desorption from clean W(110) (*22*). For all four silicon-covered

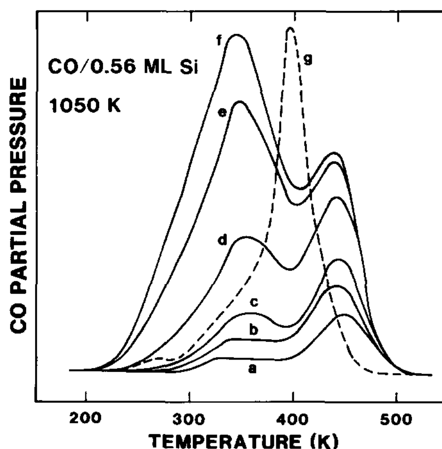

FIG. 4. Thermal desorption of CO from 0.56 ML of silicon on W(110) annealed to 1050 K. The adsorption temperature is 120 K. CO exposures are (a) 2.0, (b) 3.9, (c) 5.9, (d) 10.0, (e) 20.0, (f) 39.0 × 10^{14} molecules/cm^2. Curve g shows the saturation α-CO TPD from clean W(110) (×3/7). Heating rate = 18 K/s.

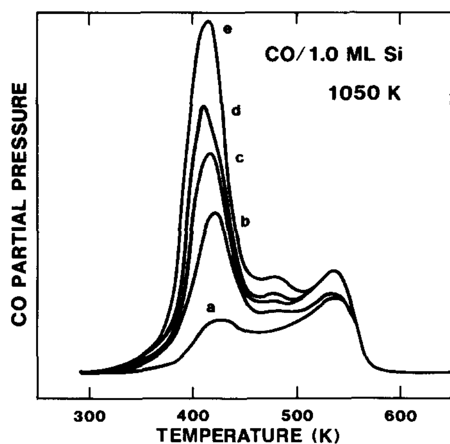

FIG. 5. Thermal desorption of CO from one monolayer of silicon on W(110), annealed to 1050 K. The adsorption temperature is 120 K. CO exposures are (a) 2.0, (b) 3.9, (c) 7.9, (d) 10.0, (e) 20.0 × 10^{14} molecules/cm^2. Heating rate = 18 K/s.

surfaces only very small amounts of hydrogen adsorb; the saturation hydrogen coverage is less than 0.05 ML in all cases. The desorption temperature of this hydrogen is less than 250 K. In contrast, the saturation coverage of hydrogen on clean W(110) is one monolayer, and the desorption temperature is 450–500 K (*22*). The anomolously low saturation coverages and desorption temperatures observed on the silicon-covered surfaces suggest that the hydrogen desorption is due to recombination of hydrogen atoms weakly bound at defect sites and boundaries between silicon domains. We therefore conclude that hydrogen dissociation is completely suppressed within the $\begin{pmatrix} 2 & 2 \\ 1 & -1 \end{pmatrix}$, $p(2 \times 2)$, $\begin{pmatrix} 4 & 4 \\ 5 & -5 \end{pmatrix}$ and $\begin{pmatrix} 6 & -1 \\ -1 & 6 \end{pmatrix}$ silicon structures.

3.3. *Benzene Adsorption*

The dissociation of C_6D_6 was studied on the six silicon-covered surfaces listed in Table 1, as well as on clean W(110). Multilayers were deposited by exposing the crystal to benzene at 120 K. The surface was then heated to 700 K to decompose benzene and remove the deuterium formed. TPD experiments indicate that benzene multilayers desorb at 180 K for all six surfaces, while D_2 formed by benzene decomposition desorbs in a broad peak at 500–700 K. A detailed TPD study was not performed. After the surface was heated to 700 K, Auger spectra were recorded to determine the relative amounts of carbon on the surface. In all cases, the carbon Auger lineshape indicates the formation of carbidic rather than graphitic carbon (*23*). In general, a single benzene exposure followed by heating is sufficient to saturate the surface with carbon and to prevent further benzene decomposition. The C(273 eV)/W(169 eV) Auger ratios observed following benzene TPD are listed in Table 1. Note that the ratios in Table 1 do not accurately reflect carbon coverages, since the W(169 eV) signal is attenuated by the addition of silicon. Thus, the carbon coverages decrease somewhat more rapidly with silicon coverage than indicated by the ratios in Table 1. For all three silicon coverages, the amount of benzene decomposition does not differ appreciably between the surfaces annealed to 700 and those annealed to 1050 K.

The LEED patterns of the silicon overlayers were altered by the deposition of carbon on the surface. For the clean surface, a (15 × 3)R14° pattern is observed after benzene decomposition. This pattern is identical to that observed following acetylene decomposition on W(110) and has been interpreted as being due to a reconstruction of the W(110) surface to form surface carbides (*24, 25*). For 0.25 ML of silicon, benzene decomposi-

TABLE 1

Carbon Deposition from Benzene Decomposition

Si coverage (ML)	C(272 eV)/W(169 eV)	
	700 K anneal	1050 K anneal
0.00	0.43	0.43
0.25	0.27	0.32
0.50	0.19	0.15
1.00	0.00	0.00

tion destroys the $\begin{pmatrix} 1 & 1 \\ 2 & -2 \end{pmatrix}$ and silicide patterns observed in the absence of carbon, resulting in diffuse (1 × 1) LEED patterns in both cases. For 0.5 ML of silicon annealed to 700 K, the $\begin{pmatrix} 2 & 2 \\ 1 & -1 \end{pmatrix}$ pattern becomes disordered after benzene decomposition, and a large increase is observed in the background signal. Decomposition of benzene on the $\begin{pmatrix} 4 & 4 \\ 5 & -5 \end{pmatrix}$ structure formed by 0.5 ML of silicon annealed to 1050 K results in increased background in the LEED pattern, but the $\begin{pmatrix} 4 & 4 \\ 5 & -5 \end{pmatrix}$ spots remain quite sharp. For a monolayer of silicon, no benzene decomposition is observed and the LEED patterns are unchanged following TPD.

3.4. Cyclohexane Dehydrogenation and Hydrogenolysis

Reactions of cyclohexane with hydrogen were studied at 630 K with 100 Torr H_2 and 1 Torr cyclohexane. In preliminary experiments using hydrogen as received, no dehydrogenation or hydrogenolysis of cyclohexane was observed on a tungsten surface covered by one monolayer of silicon annealed to 1050 K. It was found by postreaction AES, however, that the silicon-modified tungsten surface had become heavily oxidized during reaction. The silicon AES transition shifted from 92 to 76 eV, and the lineshape changed in a manner consistent with formation of SiO_2 (*23*). Furthermore, the shape of the O(510 eV) AES peak was very different from that observed for an oxidized W(110) surface. All of these observations indicate quantitative oxidation of the silicon to SiO_2. Studies of tungsten silicide oxidation have shown that oxidation occurs by diffusion of silicon to the silicide surface, resulting in formation of a passivating SiO_2 layer on top of pure tungsten metal (*26–28*). Since this passivating layer completely blocks access of reactant molecules to the tungsten atoms, and since SiO_2 alone is not a catalyst for hydrocarbon reactions, no reaction is observed on the oxidized silicide surface.

By further purifying the hydrogen to remove traces of O_2 and water, as described in the experimental section, it was possible to reduce the extent of oxidation such that only 35–75% of the silicon on the surface was transformed into SiO_2 during reaction. The extent of oxidation was measured by comparing the O(510 eV)/W(169 eV) AES ratio after reaction to the O(510 eV)/W(169 eV) ratio from a completely oxidized silicon monolayer. Lowering the total reactant pressure to 20 Torr did not reduce the extent of oxidation, indicating that the oxidizing impurities are not being introduced with the reactants. Instead, the source of the oxidizing impurities is believed to be displacement of water, oxygen, CO, etc., from the reactor walls upon introduction of the reactants. In the study of cyclohexane dehydrogenation and hydrogenolysis of Ru(0001) (*15*) no oxidation of the catalyst was reported. Apparently any oxygen deposited on the Ru(0001) surface by impurities displaced from the reactor walls was reduced to water during reaction. For the silicide catalysts, however, oxidation of the silicon results in the formation of extremely stable Si–O bonds which cannot be reduced under the reaction conditions employed here.

The partially oxidized surfaces were found to be active catalysts for reactions of cyclohexane. TOFs for hydrogenolysis and dehydrogenation are shown in Table 2. Unlike the completely oxidized silicide surface, unoxidized tungsten silicide surfaces contain tungsten atoms which are accessible to gas phase reactant molecules (*14*) and can therefore function as catalysts. Not surprisingly, the activity of the silicide surface for cyclohexane conversion was greatest when the extent of oxidation was lowest. Since the quantity of oxidizing impurities is clearly independent of the amount of silicon present, lowering the silicon coverage below a monolayer would have resulted in a greater fraction of the silicon being oxidized. For this reason, the reactor studies were confined to surfaces with a monolayer of silicon annealed to 1050 K. Even for the monolayer surface, the fraction of silicon which was oxidized varied from 35 to 75% in an unre-

TABLE 2

Cyclohexane Dehydrogenation and Hydrogenolysis Rates[a]

$T = 630$ K, $P = 101$ Torr, $H_2:C_6H_{12} = 100:1$.

Percentage of silicon oxidized	TOF (s^{-1})	
	Benzene	Alkanes
35	0.019	—[b]
50	0.002	—[b]
62	0.002	0.0002
64	0.006	0.0030
72	—[b]	0.0004
72	—[b]	0.0006
Clean W(110)[c]	0.005	0.0040

[a] Rates are averaged over the reaction time.
[b] Conversion below detection limits.
[c] Values represent an average of several experiments.

producible manner. Because of this irreproducibility, it was not possible to accurately determine activation energies or reaction orders or even if the reaction was at steady state.

When the extent of oxidation was only 35%, an amount of benzene was formed over 10 min which corresponds to an *average* TOF of 0.019 s^{-1}. In cases where >60% of the silicon was oxidized, the amount of benzene formed corresponded to TOFs of 0.006 s^{-1} or less. With one exception, only small amounts of alkanes were formed on the silicide surface. In addition, traces of cyclohexene may have been formed, but overlap between the cyclohexene and cyclohexane peaks made quantitative determination of the cyclohexene impossible. Following reaction, submonolayer quantities of carbon were present on the surface, as detected by AES. The AES carbon lineshape indicated that the carbon was present in a carbidic form (*23*).

Also shown in Table 2 are benzene and alkane formation rates for clean W(110). The rate of benzene formation on W(110) is lower than that on the least oxidized silicide surface, while the amount of alkanes formed is clearly greater. After reaction, carbidic carbon is detected by AES and the C(273 eV)/W(169 eV) Auger ratio is 0.43. This ratio is identical to the ratio observed after benzene is decomposed on clean W(110), suggesting that tungsten carbide is formed under reaction conditions. Since LEED measurements cannot be made in the UHV chamber connected to the high-pressure reactor, it was not possible to determine if the (15 × 3)R14° pattern formed by benzene decomposition on W(110) is formed under the reaction conditions employed here.

4. DISCUSSION

In order to understand the effects of adsorbed silicon atoms on the adsorption of CO and hydrogen it is necessary to know the adsorption sites of silicon, carbon, oxygen, and hydrogen atoms and CO molecules. The four types of adsorption sites available on a W(110) surface are shown in Fig. 6. Virgin CO molecules are bound upright on the surface with the carbon end down (*29*). As the CO coverage in the virgin state is increased, a series of LEED patterns which indicates shifts in the location of the CO molecules relative to the W(110) substrate (*20*) is observed. This shifting suggests that CO adsorption in the virgin state is not site specific (*20*). Based on the surface structures proposed by Steinbruchel and Gomer (*20*), however, it would appear that adsorption at short bridge sites or atop sites is preferred, except at very high coverages. The C–O stretching frequency of 1980 cm^{-1} for virgin CO on W(110) (*30*) supports CO adsorption

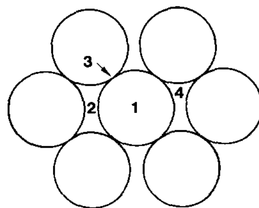

FIG. 6. Adsorption sites on W(110). (1) Atop, (2) long bridge, (3) short bridge, (4) pseudo-threefold hollow.

on either atop or bridge sites in an upright geometry. Throughout this discussion it is therefore assumed that molecular CO is adsorbed at either short bridge or atop sites.

Shustorovich (*31*) has shown theoretically that atoms adsorb preferentially in hollow or bridge sites regardless of the nature of the atomic adsorbate or the substrate. Two studies of hydrogen adsorption on W(110) have concluded that hydrogen atoms are indeed located in long bridge sites (*32, 33*), although Davies and Erskine (*33*) feel that short bridge sites are also occupied at saturation. Carbon and oxygen atoms formed by CO dissociation will also be taken to be adsorbed in long bridge sites. Note that adsorption of carbon, oxygen, and hydrogen atoms at pseudo-threefold hollow sites is also possible, but that the arguments presented in Sections 4.1 and 4.2. are applicable regardless of which adsorption site is assumed.

The location of silicon atoms has already been discussed, and the relevant surface structures are shown in Fig. 1. Based on previous work measuring silicon coverages and LEED patterns (*14*), it is believed that the silicon atoms are uniformly dispersed across the surface at all coverages above 0.25 ML. Furthermore, if islanding of silicon were occurring, such that adsorption and reaction occurred only on clean patches of tungsten between silicon islands, then CO desorption temperatures and cyclohexane dehydrogenation selectivity would be unaffected by silicon, contrary to experimental observations. Thus, the results of this study cannot be explained by adsorption of reactants on clean tungsten regions between silicon islands. Instead, a uniform distribution of silicon atoms must be assumed.

At present, the mechanism by which CO molecules dissociate on W(110) is unknown. Recent observations of a tilted or lying down precursor to CO dissociation on Fe(100) (*34, 35*), Mo(100) (*36*), and Cr(110) (*37*) suggest that CO dissociation generally requires an upright CO molecule to tilt such that both the carbon and oxygen atoms interact with the surface. In order for dissociation to proceed, the tilted CO molecule must be located near two adjacent empty atomic adsorption sites. Throughout this discussion it is therefore assumed that CO dissociation occurs by tilting of a molecularly adsorbed CO molecule across a short bridge site and requires two empty long bridge sites adjacent to the short bridge site. A similar mechanism is assumed for H_2 dissociation.

4.1. CO Adsorption

4.1.1. 0.30 ML silicon. In previous work (*14*) it was shown that as the silicon coverage increases from 0.25 to 0.50 ML, the LEED pattern observed after annealing to 700 K gradually changes from the $\begin{pmatrix}1 & 1\\ 2 & -2\end{pmatrix}$ structure (Fig. 1a) to the $\begin{pmatrix}2 & 2\\ 1 & -1\end{pmatrix}$ structure (Fig. 1b). For coverages between 0.25 and 0.5 ML both structures coexist, with the fraction of the surface covered by each structure determined by the overall silicon coverage. For 0.30 ML of silicon, therefore, approximately 80% of the surface is covered by $\begin{pmatrix}1 & 1\\ 2 & -2\end{pmatrix}$ islands with a local silicon coverage of 0.25 ML, with the remainder of the surface covered by $\begin{pmatrix}2 & 2\\ 1 & -1\end{pmatrix}$ islands with a local silicon coverage of 0.5 ML.

TPD following a saturation CO exposure to this surface results in desorption of 0.24 ML of α-CO and 0.16 ML of β-CO. Thus, 0.40 ML of virgin CO must be present on the surface immediately following the exposure. The value of 2.8 Å suggested by Kohrt and Gomer (*38*) for the diameter of an adsorbed CO molecule is nearly equal to the nearest neighbor distance on the W(110) surface (*39, 40*). Thus, examination of Fig. 1b clearly shows that steric considerations allow at most one CO molecule to be adsorbed in each unit cell of the $\begin{pmatrix}2 & 2\\ 1 & -1\end{pmatrix}$ structure. Although steric considerations alone would allow the CO molecule to be adsorbed at either atop or long bridge sites, earlier work (*20*) suggests that the atop site is more energetically favorable.

Note that Fig. 1b represents only one possible $\begin{pmatrix}2 & 2\\ 1 & -1\end{pmatrix}$ structure. It is possible to construct $\begin{pmatrix}2 & 2\\ 1 & -1\end{pmatrix}$ structures which allow two ad-

sorbed CO molecules per unit cell. These structures, however, also contain sites for CO dissociation. Since, as shown below (Section 4.1.2.), CO dissociation does not occur within the $\begin{pmatrix} 2 & 2 \\ 1 & -1 \end{pmatrix}$ islands, any $\begin{pmatrix} 2 & 2 \\ 1 & -1 \end{pmatrix}$ structures which contain sites for two CO molecules per unit cell (and therefore sites for CO dissociation) can be ruled out. Thus, we conclude that only one CO molecule can be adsorbed in each unit cell of the $\begin{pmatrix} 2 & 2 \\ 1 & -1 \end{pmatrix}$ structure. Since there are four tungsten atoms in each $\begin{pmatrix} 2 & 2 \\ 1 & -1 \end{pmatrix}$ unit cell, the maximum local CO coverage within the $\begin{pmatrix} 2 & 2 \\ 1 & -1 \end{pmatrix}$ islands is 0.25 ML. At an overall coverage of 0.30 ML, the $\begin{pmatrix} 2 & 2 \\ 1 & -1 \end{pmatrix}$ structure covers 20% of the surface, so that a total of 0.05 ML of CO can be adsorbed within the $\begin{pmatrix} 2 & 2 \\ 1 & -1 \end{pmatrix}$ islands. As a result, 0.35 ML of CO must be contained within the $\begin{pmatrix} 1 & 1 \\ 2 & -2 \end{pmatrix}$ islands. Since 80% of the surface is covered by $\begin{pmatrix} 1 & 1 \\ 2 & -2 \end{pmatrix}$ islands, the local CO coverage within the $\begin{pmatrix} 1 & 1 \\ 2 & -2 \end{pmatrix}$ islands must be approximately 0.5 ML. As for the $\begin{pmatrix} 2 & 2 \\ 1 & -1 \end{pmatrix}$ structure, the $\begin{pmatrix} 1 & 1 \\ 2 & -2 \end{pmatrix}$ structure contains four tungsten atoms per unit cell. Thus, two CO molecules must be placed in each unit cell to obtain the required coverage. Examination of the $\begin{pmatrix} 1 & 1 \\ 2 & -2 \end{pmatrix}$ structure in Fig. 1a shows that only one atop site per unit cell is unobstructed by silicon atoms. It is possible, however, to place two CO molecules within each unit cell if the CO molecules are adsorbed at short bridge sites. Furthermore, it is evident that within the $\begin{pmatrix} 1 & 1 \\ 2 & -2 \end{pmatrix}$ structure, pairs of adjacent empty long bridge sites exist which can accommodate CO dissociation, consistent with the β-CO desorption observed in Fig. 2a.

It is interesting to note that the desorption peak temperature of α-CO from a surface covered by 0.30 ML of silicon annealed to 700 K is identical, within experimental error, to the peak temperature for CO desorption from the clean surface. Also, within the $\begin{pmatrix} 1 & 1 \\ 2 & -2 \end{pmatrix}$ islands the fraction of the virgin CO which dissociates is similar to that observed on the clean W(110) surface. These results suggest that the primary effect of silicon on CO adsorption is steric in nature and does not involve severe electronic perturbation of the tungsten surface. The very similar electronegativities of silicon and tungsten (*41*) also argue against a strong electronic effect.

Upon annealing 0.30 ML of silicon to 1050 K to form the silicide, the virgin CO saturation coverage increases to 0.58 ML. During TPD, 0.50 ML of CO desorbs in the α states, while 0.08 ML of CO dissociates and desorbs as β-CO. The increase in the saturation coverage of CO upon silicide formation is easily understood. The diffusion of silicon into the tungsten surface to form the silicide increases the number of exposed tungsten atoms at the surface. Since fewer tungsten atoms are sterically blocked by silicon atoms, the number of available CO adsorption sites increases. It is somewhat surprising that the amount of β-CO which is formed is actually lowered by annealing to 1050 K. It must be remembered, however, that CO dissociation and α-CO desorption occurs simultaneously (*19, 20*). Thus, the relative amounts of CO in the α and β states are determined by competition between desorption and dissociation. Apparently the formation of the silicide alters the competition between the two processes in such a manner as to increase the fraction of CO which desorbs rather than dissociates.

4.1.2. 0.56 ML of silicon. For silicon coverages between 0.50 and 0.75 ML, both the $\begin{pmatrix} 2 & 2 \\ 1 & -1 \end{pmatrix}$ and the $\begin{pmatrix} 2 & 2 \\ 2 & -2 \end{pmatrix}$ structures coexist (*14*). At the coverage of 0.56 ML used in this work, approximately three-quarters of the surface must be covered with the $\begin{pmatrix} 2 & 2 \\ 1 & -1 \end{pmatrix}$ structure, with the rest of the surface covered by the $\begin{pmatrix} 2 & 2 \\ 2 & -2 \end{pmatrix}$ structure. Within the $\begin{pmatrix} 2 & 2 \\ 2 & -2 \end{pmatrix}$ islands, Fig. 1c shows that all atop and short bridge adsorption sites are severely hindered sterically by neighboring silicon atoms. Although other $\begin{pmatrix} 2 & 2 \\ 2 & -2 \end{pmatrix}$ structures are possible (*14*), all reasonable alternatives to the structure in Fig. 1c also result in steric hinderance of the atop and short bridge sites. Certain long bridge sites in Fig. 1c are sufficiently unhindered that adsorption of CO at these sites cannot be ruled out by steric considerations. From earlier discus-

sion, however, it would appear that CO adsorption in long bridge sites is not energetically favorable. Thus, it can reasonably be concluded that CO adsorption is completely suppressed within the $\begin{pmatrix}2 & 2\\ 2 & -2\end{pmatrix}$ islands. In Section 4.1.1., it was pointed out that the maximum local CO coverage which can be obtained within the $\begin{pmatrix}2 & 2\\ 1 & -1\end{pmatrix}$ islands is 0.25 ML. Since for a total silicon coverage of 0.56 ML approximately 75% of the surface is covered by $\begin{pmatrix}2 & 2\\ 1 & -1\end{pmatrix}$ islands, the maximum *overall* CO coverage obtained on a W(110) surface covered by 0.56 ML of silicon annealed to 700 K is 0.18 ML. This calculated maximum CO coverage is in good agreement with the experimentally determined maximum coverage of 0.21 ML. Since the effect of adsorbed silicon atoms on W(110) appears to be primarily steric in nature (Section 4.1.1.), the absence of CO dissociation on a surface covered by 0.56 ML of silicon indicates that adjacent pairs of unoccupied long bridge sites do not exist in either the $\begin{pmatrix}2 & 2\\ 1 & -1\end{pmatrix}$ or the $\begin{pmatrix}2 & 2\\ 2 & -2\end{pmatrix}$ structures. Thus, although many structures could give rise to $\begin{pmatrix}2 & 2\\ 1 & -1\end{pmatrix}$ and $\begin{pmatrix}2 & 2\\ 2 & -2\end{pmatrix}$ LEED patterns, only those structures which block all pairs of adjacent long bridge sites are consistent with the CO chemisorption data.

There are two major peaks in the CO desorption spectrum shown in Fig. 3. These two peaks occur at temperatures of 325 and 440 K, neither of which corresponds to the α-CO desorption observed on clean W(110). The higher temperature peak has been observed previously by Hashimoto *et al.* (*6*) on a silicon-covered polycrystalline tungsten surface. In that work the increase in desorption temperatures was attributed to a decrease in the amount of CO which dissociates in the presence of silicon. It was postulated that the carbon and oxygen atoms formed by dissociation, being more electronegative than tungsten, withdraw charge from the surface. This charge withdrawal decreases the ability of the tungsten surface to stabilize molecular CO adsorption through pi backbonding and thereby accelerates the rate of α-CO desorption. When CO dissociation is blocked by the presence of silicon, this acceleration does not occur and the α-CO desorption peak temperature increases. Note that for 0.30 ML of silicon (Section 4.1.1.) dissociation of CO does occur, resulting in an α-CO desorption temperature which is very close to that observed on clean W(110).

Hashimoto *et al.* (*6*) did not observe a CO desorption peak near 350 K, possibly because CO molecules in the low-temperature state are not stable to desorption at the relatively high adsorption temperature of 292 K used in that work. The origin of the 350 K peak is not understood at present. The shoulder at 280 K in Fig. 3 is also observed for CO desorption from clean W(110), perhaps indicating that this peak is due to CO adsorbed at defect sites.

After annealing 0.56 ML of silicon to 1050 K to form a silicide, the ability of the surface to adsorb CO increases from 0.21 to 0.50 ML. The positions of the two major CO desorption peaks are not altered by silicide formation, but the relative populations in the two peaks do change. This result suggests that similar adsorption sites are present on both surfaces, but that annealing alters the relative population of the two sites. As was the case for 0.30 ML of silicon, the increase in the capacity of the surface to adsorb CO upon annealing to 1050 K is due to diffusion of silicon into the substrate to form tungsten silicide, thereby increasing the number of exposed tungsten atoms at the surface. Dissociation of CO is still suppressed after annealing to 1050 K, indicating that the $\begin{pmatrix}4 & 4\\ 5 & -5\end{pmatrix}$ silicide surface structure does not contain appropriate sites for CO dissociation.

4.1.3. 1.0 ML of silicon. Steric arguments similar to those advanced above to explain CO adsorption on 0.30 and 0.56 ML of silicon also explain the effects of a monolayer of silicon on CO adsorption. A monolayer of silicon annealed to 700 K forms a disordered $p(2 \times 2)$ structure (Fig. 1d). The disorder is due to diffusion of a small amount of the silicon into the substrate, resulting in a less

than optimum coverage for the $p(2 \times 2)$ pattern on the surface. Within the $p(2 \times 2)$ structure there are clearly no atop or short bridge sites which are not sterically hindered by neighboring silicon atoms. Thus, no adsorption, either molecular or dissociative, is expected within the $p(2 \times 2)$ structure. Since disordering of the $p(2 \times 2)$ overlayer upon annealing to 700 K might be expected to create sites for CO adsorption, the absence of significant CO adsorption suggests that the extent of the disorder is small.

After annealing a monolayer of silicon to 1050 K, the CO adsorption capacity increases to about 0.15 ML. As for 0.30 and 0.56 ML of silicon, this increase in CO adsorption is attributed to diffusion of silicon into the substrate, thereby exposing tungsten atoms which were previously covered by silicon. Dissociation of CO was still completely suppressed after annealing to 1050 K, as evidenced by the absence of any CO desorption above 900 K.

Two desorption peaks are apparent in Fig. 5 at 480 and 540 K. The somewhat higher desorption temperatures of these peaks relative to that of clean W(110) can be explained by arguments similar to those presented in Section 4.1.2. and Ref. (*6*) for CO desorption from partially silicon-covered tungsten surfaces. The position of the main CO desorption peak at 400 K is very close to the desorption temperature of α-CO from clean W(110). On the clean W(110) surface, however, desorption may be accelerated by CO dissociation (*6*). This acceleration is absent on the silicide surface since no CO dissociation occurs. Thus, even though the desorption temperatures are similar in the two cases, the binding energy of CO on clean W(110) may nevertheless be higher than that on the $\begin{pmatrix} 6 & -1 \\ -1 & 6 \end{pmatrix}$ silicide surface.

4.1.4. Comparison with previous work. It is of interest to compare the present results for CO adsorption on silicon-covered W(110) with the work of Hashimoto *et al.* (*6*) on silicon-covered polycrystalline tungsten. While silicon results in inhibition of CO adsorption on both surfaces, the variation of the saturation CO coverage with silicon coverage differs greatly. On polycrystalline tungsten the β-CO desorption decreases as $(1 - \theta_{Si})^2$, while the α-CO desorption decreases as $(1 - \theta_{Si})$ (θ_{Si} is the silicon coverage). In contrast, on W(110) β-CO adsorption is completely poisoned by the presence of 0.56 ML of silicon and variation of the saturation α-CO coverage with θ_{Si} deviates significantly from a $(1 - \theta_{Si})$ dependence. The effect of silicon coverage on CO adsorption on polycrystalline tungsten clearly indicates a random distribution of the silicon atoms (*6*). On W(110), however, the silicon atoms adsorb in ordered overlayer structures, resulting in a faster decrease in the number of unblocked CO adsorption sites than is observed on polycrystalline tungsten.

Comparison of the adsorption of CO on the tungsten silicide surfaces with adsorption of CO on $NiSi_2(111)$ (*8*) raises a number of intriguing points. On nickel disilicide, molecular CO has a very low sticking probability even at 170 K. Once adsorbed, however, CO molecules dissociate rapidly at 170 K. It is surprising that silicide formation decreases the ability of tungsten to dissociate CO, while the ability of nickel to dissociate CO is dramatically increased by silicide formation. In addition, on W(110) the presence of silicon lowers the capacity of the surface to adsorb CO, but does not noticeably reduce the sticking probability. In contrast, the sticking probability of CO on nickel disilicide is much lower than that on clean nickel surfaces (*8*). Thus, the effect of silicide formation on the chemisorption of CO is quite different for tungsten than for nickel.

4.2. Hydrogen Adsorption

Hydrogen adsorption is almost completely suppressed by the presence of 0.5 or 1.0 ML of silicon, regardless of the annealing temperature. This suppression is analogous to the suppression of dissociative CO adsorption. Within the $\begin{pmatrix} 2 & 2 \\ 1 & -1 \end{pmatrix}$ $\begin{pmatrix} 2 & 2 \\ 2 & -2 \end{pmatrix}$ and $p(2 \times 2)$ structures shown in Fig. 1 the sites necessary for dissociative adsorption of hy-

drogen are completely blocked by silicon atoms. The small amounts of hydrogen dissociation which are observed probably occur at defect sites or domain boundaries within the silicon overlayers.

The adsorption of hydrogen on nickel disilicide is quite similar to that on the tungsten silicide surfaces (*8*). In both cases, the silicides show little or no ability to dissociate H_2. In a comparison of chemisorption on tungsten and nickel silicides, it is intriguing to note that CO chemisorption is very different on the two silicides, while hydrogen adsorption shows a marked similarity. Further comparison of the chemisorptive properties of various metal silicides might therefore be an interesting area of research.

4.3. Benzene Adsorption

To date no studies appear to have been published on benzene adsorption on W(110). The results reported here are, however, in qualitative agreement with studies of benzene adsorption on other transition metal surfaces (*42–44*). Benzene undergoes extensive decomposition on W(110), releasing hydrogen during thermal desorption in a broad peak at 500–700 K. The resulting carbon species react with the tungsten surface to form tungsten carbide.

From Table 1 it can be seen that the C(272 eV)/W(169 eV) ratio decreases approximately linearly with silicon coverage, regardless of the temperature to which the silicon is annealed prior to benzene adsorption. As discussed in Section 3.3, however, the carbon coverage decreases faster than the C(272 eV)/W(169 eV) ratio due to attenuation of the W(169 eV) signal by silicon. Thus, only qualitative statements regarding the poisoning of benzene dissociation by silicon can be made. The fact that benzene decomposition can be observed at a silicon coverage of 0.5 ML indicates that benzene dissociation is not affected by silicon as severely as CO and H_2 dissociation. Nevertheless, silicon does have a strong effect on benzene dissociation, and the data indicate that complete inhibition of benzene decomposition probably occurs at a silicon coverage somewhat less than one monolayer.

The deposition of carbon disrupts the structure of the silicon-covered surfaces. For some surfaces, the silicon overlayer structures are destroyed, while on other surfaces the silicon structures are left intact but a disordered carbon layer is formed.

4.4. Catalysis on Silicon-Modified W(110)

As stated in the introduction, tungsten is generally a poor catalytic material because of its extremely high reactivity. Consequently, in order to make a useful tungsten-based catalyst, this high reactivity must be moderated. By adsorbing silicon on the W(110) surface, the chemisorptive properties of W(110) can be altered dramatically. By varying the silicon coverage between 0.0 and 1.0 ML it is possible to go from a surface which readily dissociates molecules such as CO, H_2, and benzene to a surface which is completely inert for dissociation of all of these molecules. This ability to moderate the chemisorptive properties of W(110) by silicon addition suggests that it might also be possible to moderate the catalytic properties of tungsten in a similar manner.

The dehydrogenation and hydrogenolysis of cyclohexane were used to test the catalytic activity of silicon-modified W(110). This particular reaction was chosen for several reasons. First, in a recent study of cyclohexane dehydrogenation and hydrogenolysis on supported nickel catalysts (*9*) it was found that pretreatment of supported nickel catalysts with various silanes results in high selectivity toward dehydrogenation. This high selectivity was attributed to the fact that dissociative chemisorption of H_2 is much less favorable on nickel disilicide than on pure nickel (*8*). As a result, hydrogenolysis reactions are inhibited while dehydrogenation is relatively unaffected. By studying the same reaction on a different metal surface, it should be possible to determine if this enhanced selectivity is unique to nickel catalysts or is a general property of silicon-modified metal surfaces. Second, the inhibi-

tion of benzene decomposition by adsorbed silicon indicates that benzene formed by cyclohexane dehydrogenation on a silicon-modified tungsten surface would preferentially desorb rather than undergo further dehydrogenation to form adsorbed carbon and hydrogen atoms, thereby increasing the yield of dehydrogenation products. Third, a recent study has reported on the catalytic activity of Ru(0001) for cyclohexane dehydrogenation and hydrogenolysis (*15*). Comparison of the results for tungsten silicide with those for Ru(0001) would provide a direct determination of the activity of tungsten silicide relative to that of a group VIII metal.

The unfortunate problems with oxidation of the silicon during reaction prevented a detailed study of the kinetics of cyclohexane dehydrogenation on silicon-modified W(110). Some important qualitative information was obtained, however. From Table 2 it can be seen that when the extent of silicon oxidation is only 35%, the silicide surface is more active and more selective for benzene formation than the clean W(110) surface. This result is similar to that observed for silane-treated nickel catalysts (*9*) which are as active as untreated nickel catalysts for cyclohexane dehydrogenation, but show negligible activity for cyclohexane hydrogenolysis. Thus, like silane-treated nickel, tungsten silicide is a highly selective catalyst for cyclohexane dehydrogenation.

For the experiment in which only 35% of the silicon became oxidized during reaction, the amount of benzene formed corresponds to a TOF of 0.019 s^{-1}. This number is a lower limit on the actual TOF of the tungsten silicide surface since the rate of benzene formation decreases with the extent of oxidation of the silicon. Under identical reaction conditions, the TOF for benzene formation on Ru(0001) is also approximately 0.02 s^{-1} (*15*). Thus, a W(110) surface covered by a monolayer of silicon annealed to 1050 K appears to be at least as active as Ru(0001) for cyclohexane dehydrogenation. The Ru(0001) surface is, of course, a more active hydrogenolysis catalyst.

The detection of carbidic carbon on the surface following reaction indicates that the catalyst is not pure tungsten silicide under reaction conditions. Instead, the catalyst is a combination of tungsten silicide and either tungsten carbide or silicon carbide. Based on Auger spectra alone, it is not possible to tell whether the carbide signal is due to silicon carbide or tungsten carbide. The formation of surface carbides during catalytic reactions of hydrocarbons is a general phenomenon (*15, 45*).

The sensitivity of silicon-modified tungsten catalysts to oxidation is clearly an undesirable characteristic for a catalyst. In practical catalytic processes small amounts of oxidizing species, such as water, oxygen, and CO, are often present. Thus, continuous deactivation of tungsten silicide catalysts would be expected due to irreversible oxidation of the silicon. For a low-surface-area catalyst, such as the tungsten single crystal used here, rapid deactivation of the entire active surface is expected. For a high-surface-area supported catalyst, however, the rate of oxidation might be slow enough to make practical application of tungsten silicide catalysts possible. In a packed bed reactor, for example, the section of the catalyst bed closest to the reactor inlet would become oxidized first, thereby removing the oxidizing impurities from the reactant mixture and preventing oxidation of the catalyst further downstream. Depending on impurity concentrations and catalyst surface area, it is conceivable that the rate at which the boundary between the oxidized and active sections of the catalyst bed moves through the reactor would be low enough to make the use of tungsten silicide catalysts practical. The fact that Nuzzo *et al.* (*9*) report no deactivation of their catalysts, even over periods as long as 24 h, supports the hypothesis that oxidation by trace impurities is not an insurmountable problem for high-surface-area silicon-modified catalysts.

Obviously, the sensitivity of tungsten silicide catalysts to oxidation rules out their use in reactions involving oxygen-contain-

ing molecules, such as CO methanation and oxidation reactions. Imamura and Wallace (*10, 11*) have studied CO methanation over nickel, cobalt, and iron silicides and find that oxidation of the catalysts during reaction transforms the silicides into pure metal particles supported on silica. Based on the experiments reported here, similar behavior would be expected for tungsten silicide. The formation of supported metal particles by oxidation of silicides may, however, produce methanation catalysts with qualities superior to those synthesized by more conventional techniques (*10, 11*).

5. CONCLUSION

The chemisorption of CO, H_2, and benzene on silicon-covered W(110) surfaces has been studied. The ability of the W(110) surface to dissociate these molecules can be varied greatly by changing the amount of silicon present on the surface. The poisoning of CO, H_2, and benzene adsorption and dissociation by silicon has been interpreted in terms of the known overlayer structures of silicon on W(110). This interpretation is based solely on steric considerations, indicating that electronic effects are not of primary importance for modification of tungsten surfaces by silicon. This conclusion is consistent with the small difference in electronegativity between tungsten and silicon (*41*). Annealing silicon overlayers to 1050 K to produce tungsten silicides increases the capacity of the surfaces to adsorb molecular CO. This increase is due to diffusion of silicon into the substrate upon annealing, thereby exposing additional tungsten atoms at the surface.

The ability to tailor the chemisorptive properties of W(110) by addition of silicon suggests that it might be possible to tailor the catalytic activity of W(110) as well. The dehydrogenation and hydrogenolysis of cyclohexane were used to test the catalytic activity of silicon-modified W(110). Although the interpretation of the reaction studies was complicated by partial oxidation of the catalysts during reaction, two qualitative conclusions were obtained. First, a W(110) surface covered by a monolayer of silicon annealed to 1050 K to form tungsten silicide is a highly selective dehydrogenation catalyst. Only traces of hydrogenolysis products are formed on this surface. Combined with an earlier study of cyclohexane reactions on silane-treated nickel catalysts (*9*), this work demonstrates that high selectivity for dehydrogenation is a general phenomenon for silicon-modified metal surfaces. Second, the rate of dehydrogenation of cyclohexane to benzene on tungsten silicide appears to be at least as fast as that on Ru(0001). Thus, modification of tungsten surfaces by silicon could result in catalysts which are as active as, yet more selective than, group VIII catalysts currently in use as hydrocarbon processing catalysts. The potential to replace group VIII metal catalysts with catalysts based on cheaper and more readily available materials could result in significant reductions in the cost of processing hydrocarbons.

ACKNOWLEDGMENTS

We acknowledge with pleasure the partial support of this work by the Department of Energy, Office of Basic Energy Sciences, Division of Chemical Sciences.

REFERENCES

1. Levy, R. B., and Boudart, M., *Science* **181,** 547 (1973).
2. Boudart, M., Oyama, S. T., and Leclerc, L., *in* "Proc. Seventh Int. Cong. Catal." (T. Seiyama and K. Tanabe, Eds.), Elsevier, New York, 1981.
3. Aboul-Gheit, A. K., Mendufy, M. F., and Ebeid, F. M., *Appl. Catal.* **4,** 181 (1982).
4. Volpe, L., and Boudart, M., *J. Solid State Chem.* **59,** 332 (1985).
5. Udovic, T. J., Kelley, R. D., and Madey, T. E., *Surf. Sci.* **150,** L71 (1980).
6. Hashimoto, H., Matsushima, T., and Matsui, T., *Surf. Sci.* **148,** 252 (1984).
7. Boudart, M., *in* "Critical Materials Problems in Energy Production" (C. Stein, Ed.), Academic Press, New York, 1976.
8. Dubois, L. H., and Nuzzo, R. G., *J. Amer. Chem. Soc.* **105,** 365 (1983).
9. Nuzzo, R. G., Dubois, L. H., Bowles, N. E., and Trecoske, M. A., *J. Catal.* **85,** 267 (1984).
10. Imamura, H., and Wallace, W. E., *J. Phys. Chem.* **83,** 3261 (1979).

11. Imamura, H., and Wallace, W. E., *J. Phys. Chem.* **83,** 2009 (1979).

12. Bonny, A., Brewster, R., and Wellborn, A., *Inorg. Chim. Acta* **64,** L3 (1982).

13. Fryberger, T. B., Grant, J. L., and Stair, P. C., *Langmuir* **3,** 1015 (1987).

14. Sault, A. G., and Goodman, D. W., *Surf. Sci.* **235,** 28 (1990).

15. Peden, C. H. F., and Goodman, D. W., *J. Catal.* **104,** 347 (1987).

16. Goodman, D. W., Yates, J. T., Jr., and Peden, C. H. F., *Surf. Sci.* **164,** 417 (1985).

17. Campbell, C. T. and Valone, S. M., *J. Vac. Sci. Technol., A* **3,** 408 (1985).

18. Goodman, D. W., *Acc. Chem. Res.* **17,** 194 (1984).

19. Leung, C., Vass, M., and Gomer, R., *Surf. Sci.* **66,** 67 (1977).

20. Steinbruchel, Ch., and Gomer, R., *Surf. Sci.* **67,** 21 (1977).

21. Bowker, M., and King, D. A., *J. Chem. Soc. Faraday Trans. 1* **76,** 758 (1980).

22. Tamm, P. W., and Schmidt, L. D., *J. Chem. Phys.* **54,** 4775 (1971).

23. Davis, L. E., MacDonald, N. C., Palmberg, P. W., Raich, G. E., and Weber, R. E., "Handbook of Auger Electron Spectroscopy," 2nd ed. Perkin–Elmer, Eden Prairie, MN, 1978.

24. Ollis, D. F., and Boudart, M., *Surf. Sci.* **23,** 320 (1970).

25. Rawlings, K. J., Foulias, S. D., and Hopkins, B. J., *J. Phys. C* **14,** 5411 (1981).

26. Zirinsky, S., Hammar, W., d'Huerle, F. M., and Baglin, J., *Appl. Phys. Lett.* **33,** 76 (1978).

27. Baglin, J. E., d'Huerle, F. M., and Petersson, C. S., *Appl. Phys. Lett.* **33,** 289 (1978).

28. Gelain, C., Cassuto, A., and LeGoff, P., *Oxid. Met.* **3,** 153 (1971).

29. Madey, T. E., Houston, J. E., and Dahlberg, S. C., *in* "Proc. Fourth Int. Conf. Solid Surfaces and Third European Conf. on Surface Sci." (D. A. Degras and M. Costa, Eds.), Vol. 1, p. 205. Supplement a la Revue "Le Vide, les Couches Minces," No. 201, 1980.

30. Backx, C., Willis, R. F., Feuerbacher, B., and Fitton, B., *Surf. Sci.* **68,** 516 (1977).

31. Shustorovich, E., *Surf. Sci. Rep.* **6,** 1 (1986).

32. Blanchet, G. B., Dinardo, N. J., and Plummer, E. W., *Surf. Sci.* **118,** 496 (1982).

33. Davies, B. M., and Erskine, J. L., *J. Electron Spectrosc. Relat. Phenom.* **29,** 323 (1983).

34. Fadley, C. S., *in* "Tenth Taniguchi International Symposium on Core Level Spectroscopy in Condensed Systems, Shima, Japan, October 18–23, 1987."

35. Moon, D. W., Bernasek, S. L., Gland, J. L., and Dwyer, D. J., *Surf. Sci.* **184,** 90 (1987).

36. Zaera, F., Kollin, E., and Gland, J. L., *Chem. Phys. Lett.* **121,** 464 (1985).

37. Shinn, N. D. and Madey, T. E., *Phys. Rev. Lett.* **53,** 2481 (1984).

38. Kohrt, C., and Gomer, R., *Surf. Sci.* **24,** 77 (1971).

39. Cullity, B. D., "Elements of X-Ray Diffraction," p. 506. Addison–Wesley, Menlo Park, CA, 1978.

40. Weast, R. B. (Ed.), "Handbook of Chemistry and Physics," 68th ed. CRC Press, Boca Raton, FL, 1987.

41. Pauling, L., "The Nature of the Chemical Bond," 3rd ed. Cornell Univ. Press, Ithaca, NY, 1960.

42. Alnot, M., Ducros, R., Ehrhardt, J. J., and Tatarenko, S., *Appl. Surf. Sci.* **14,** 114 (1983).

43. Friend, C. M., and Muetterties, E. L., *J. Amer. Chem. Soc.* **103,** 773 (1981).

44. Tsai, M.-C., and Muetterties, E. L., *J. Amer. Chem. Soc.* **104,** 2534 (1982).

45. Sault, A. G., and Goodman, D. W., *in* "Molecule–Surface Interactions" (K. Lawley, Ed.), Wiley, New York, 1989.